ELSEVIER

Tectonophysics 265 (1996) 83–100

TECTONOPHYSICS

Evolution of deep-crustal normal faults: constraints from thermobarometry in the Grenville Orogen, Ontario, Canada

Jay P. Busch [a], Eric J. Essene [a], Ben A. van der Pluijm [a,*]

[a] *Department of Geological Sciences, 2534 C.C. Little Bldg., University of Michigan, Ann Arbor, MI 48109-1063, USA*

Received 21 March 1995; accepted 8 December 1995

Abstract

The Robertson Lake shear zone (RLSZ) is a low-angle (~30° dip), plastic to brittle extensional shear zone located in the southeastern Grenville Orogen, Ontario, Canada. Thermobarometric data have been collected to evaluate the effects of extension on regional metamorphic field gradients. Upper greenschist facies metamorphic conditions are preserved in the footwall and upper amphibolite facies metamorphic conditions in the hanging wall. However, steep gradients in metamorphic pressure are present adjacent to the Robertson Lake shear zone. In the footwall pressures increase from 550 MPa to 800 MPa within 8 km of the RLSZ and in the hanging wall pressures decrease from 900 MPa to 500 MPa within 12 km of the RLSZ. The pressure gradients are interpreted to be a product of isostatic flexural rotations in response to extension along the zone. The degree of rotation indicated by the baric gradients in the hanging wall and footwall are compatible and require an initial shear zone orientation of 60–90°, which suggests reactivation of an initially high-angle terrane boundary. Previous studies provide constraints of a depth extent of 40 km for the RLSZ and crustal thickness of 60 km during extension. Thus, extensional rotations were accommodated by decoupling and regional-scale flow in the lower third of the crust.

Keywords: structural analysis; petrology; regional metamorphism; Ontario; extension tectonics; Grenville Province; shear zones

1. Introduction

Styles of extension have been defined in many extended terranes based on constraints from originally horizontal marker beds, fault orientations, and seismic data. These studies have generally been restricted to the upper crust in active or relatively young tectonic settings (e.g., McKenzie, 1978; Davis, 1983; Jackson, 1987; Jackson et al., 1988; Davidson, 1989). In these settings the integration of surface geology with seismic observations has provided a description of the geometries of faults, fault blocks, and their geometric evolution (style) during extension. In deeply eroded extensional terranes, fault zones are typically crystal–plastic mylonite zones developed in metamorphic rocks (Brodie and Rutter, 1987; Carlson et al., 1990; Andersen and Jamtveit, 1990). These terranes lack syn-orogenic sedimentary rocks and stratigraphic control, so that field studies generally do not provide geometrical constraints on extensional style. The approaches used in high-grade metamorphic ter-

* Corresponding author. e-mail: vdpluijm@umich.edu.

PII S0040-1951(96)00147-3

ranes generally focus on the effects of extension on pressure–temperature paths or temperature–time paths of the extending crust with little reference to geometry (Brodie and Rutter, 1987; Ruppel et al., 1988; Cosca et al., 1992; Hodges et al., 1993; van der Pluijm et al., 1994). The style of extension in the deep crust must be inferred by analogy to shallow crustal levels or from conceptual models and theoretical studies (e.g., Barr, 1987; Buck, 1988; Wernicke and Axen, 1988; Block and Royden, 1990) due to the lack of geometric constraints.

Description of the style of deep-crustal extension is pertinent to our understanding of deep-orogenic processes and assessing the degree of mechanical coupling of upper- and lower-crustal rocks during deformation. Workers in the Basin and Range Province have suggested that the lower crust deforms by regional-scale plastic flow to accommodate extension and is decoupled from the brittlely deformed upper crust (Stewart, 1971; Miller et al., 1983; Smith and Bruhn, 1984; Gans et al., 1985; Gans, 1987; Block and Royden, 1990). If the deep crust is decoupled from the shallow crust, descriptions of extensional styles based on unmetamorphosed cover rocks have limited bearing on the geometry of deep-crustal processes. Numerous field studies have documented the existence of low-angle normal faults (decoupling horizons) and a variety of hypotheses have been proposed to explain the mechanics of low-angle normal faults (Shackelford, 1980; Wernicke, 1981; Brun and Choukroune, 1983; Spencer and Chase, 1989; Scott and Lister, 1992; Parsons and Thompson, 1993; Reynolds et al., 1994). However, as yet there is no consensus on the mechanics of crustal extension. The majority of these studies are from the Basin and Range Province and the general applicability of these models is uncertain.

In the Grenville Province, the root of a Middle Proterozoic mountain belt is exposed. Structures in the Grenville Province of North America are generally considered to be a middle- to lower-crustal expression of thrust tectonics (Davidson, 1984; Hanmer, 1988; Rivers et al., 1989; McEachern and van Breemen, 1993). Extensional deformation associated with the last phase in the Grenville orogenic cycle has been recognized (van der Pluijm and Carlson, 1989; Mezger et al., 1991; Culshaw et al., 1994; Cureton, 1994; Busch and van der Pluijm, 1996). These studies illustrate that extension is a significant component of the tectonic evolution of the Grenville Orogen.

The Robertson Lake Shear Zone (RLSZ) is a low-angle extensional shear zone which separates two domains within the eastern Metasedimentary Belt (Fig. 1). The RLSZ is a crystal plastic mylonite zone that dips 30° to the southeast and contains abundant, normal shear-sense indicators developed over the plastic to brittle transition (Busch and van der Pluijm, 1996). Mylonites are overlain and overprinted by a zone of cataclastic deformation that marks the transition into the hanging wall. This paper focuses on regional gradients in metamorphic pressure and temperature, and metamorphic discontinuities across the RLSZ. The metamorphic data are used to define the style of extension, constrain the pre-extension shear zone orientation, and evaluate the geodynamic significance of the RLSZ.

2. Regional geology

The Metasedimentary Belt is composed of marble, clastic metasedimentary rocks, and a variety of plutonic and volcanic rocks. It has been divided into five lithotectonic domains based on geophysical, lithologic and chronological data (Easton, 1992). The RLSZ separates the Sharbot Lake and Mazinaw domains (Fig. 1a). The Mazinaw domain is dominated by deformed granite and tonalite plutonic rocks, clastic metasedimentary rocks (quartzofeldspathic schist, gneiss and mica schist), and metavolcanic rocks (amphibole schist) metamorphosed at upper greenschist to amphibolite facies conditions (e.g., Anovitz and Essene, 1990). Based on metamorphic mineral assemblages, an increase in metamorphic grade from west to east has been documented in the Mazinaw domain (Fig. 1b; Hutcheon and Moore, 1973; Sethuraman and Moore, 1973; Thompson, 1973; Carmichael et al., 1978; Moore and Thompson, 1980). Metamorphic studies generally indicate peak metamorphic pressures of 400–600 MPa and temperatures of 400–600°C in the central Elzevir and central Mazinaw domains (Hutcheon and Moore, 1973; Dunn and Gilliam, 1994; Cureton, 1994). Temperatures calculated from chemical data of Thompson and Leclair (1987) and Hounslow and Moore (1967) on garnet and biotite provide addi-

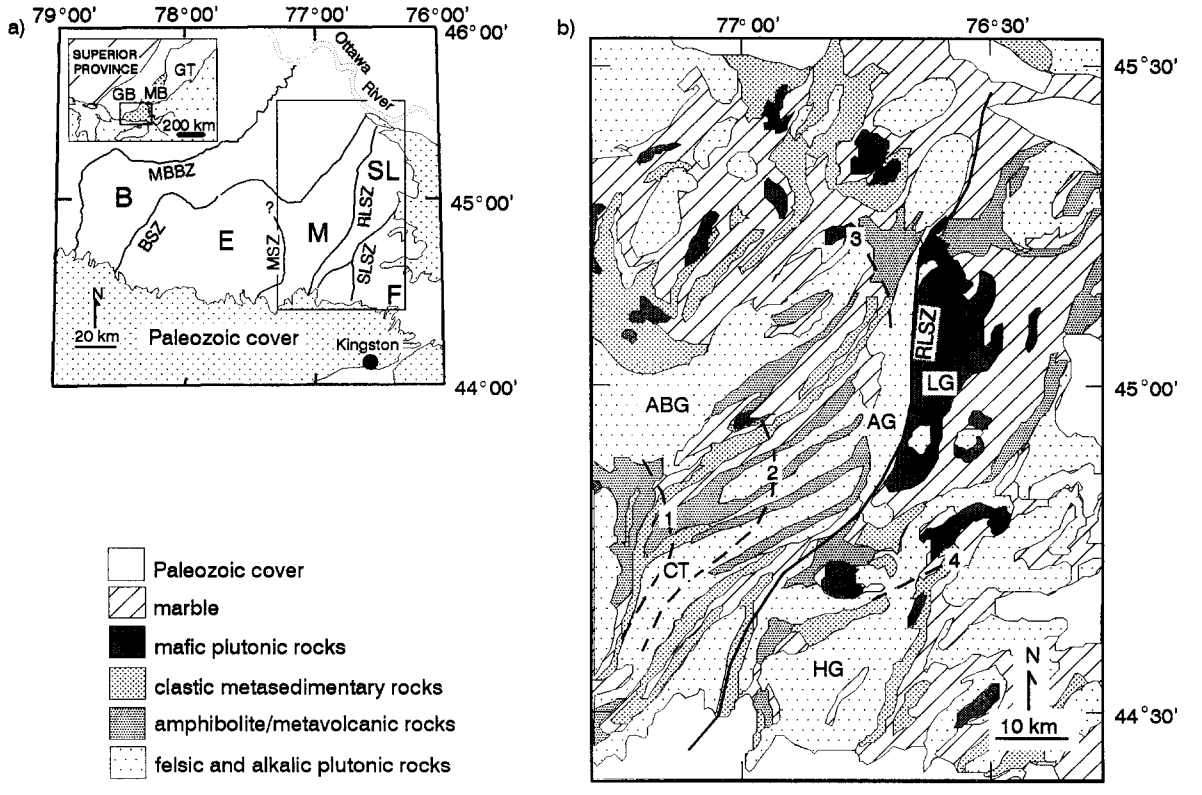

Fig. 1. (a) General subdivisions of the Metasedimentary Belt (modified from Ontario Geological Survey, 1992b): *B* = Bancroft domain; *E* = Elzevir domain; *M* = Mazinaw domain; *SL* = Sharbot Lake domain; *F* Frontenac domain; *MBBZ* = Metasedimentary Belt Boundary Zone; *BSZ* = Bancroft Shear Zone; *MSZ* = Mooroton Shear Zone; *RLSZ* = Robertson Lake Shear Zone; *SLSZ* = Sharbot Lake Shear Zone. Light stipple is Paleozoic cover. Inset shows major subdivisions of the Grenville Orogen in Canada. *GB* = granulite belt; *MB* = metasedimentary belt; *GT* = granulite terrane. Box outlines area of (b) and Fig. 3. (b) Geologic map (modified from Ontario Geological Survey, 1992a) with isograds (dashed lines). Isograds are (*1*) staurolite, (*2*) sillimanite, (*3*) K-feldspar, and (*4*) pyroxene, with higher grades toward the east and southeast (from Carmichael et al., 1978). Abbreviations: *LG* = Lavant gabbro; *HG* = Hinchinbrooke gneiss; *AG* = Addington granite; *CT* = Cross Lake tonalite; *ABG* = Abinger granite.

tional temperature data of 400 to 550°C in the central Metasedimentary Belt. Additional pressure data (550–610 MPa) in the southern Mazinaw domain were obtained by Rathmell (1993) and calculated from compositional data of Cureton (1994).

The oldest rocks of the Mazinaw domain have crystallization ages between 1240 and 1270 Ma (van Breemen and Davidson, 1988; Lumbers et al., 1990; Corfu and Easton, 1994). The overlying Flinton Group clastic metasedimentary, marble and metavolcanic rocks were originally deposited after 1150 Ma (Sager-Kinsman and Parrish, 1993). Three metamorphic events probably associated with accretion of the Metasedimentary Belt to the Gneiss Belt (ca. 1190 Ma), collisional reactivation of the Metasedimentary Belt boundary zone (1080–1060 Ma) and an event with associated syn-orogenic collapse (1012–1094 Ma) affected these rocks (Mezger et al., 1991; Easton, 1992; McEachern and van Breemen, 1993; Mezger et al., 1993; Corfu and Easton, 1995). Hornblende and biotite $^{40}Ar/^{39}Ar$ cooling ages indicate that the Mazinaw domain cooled through ~500°C and ~300°C at ~940 Ma and ~900 Ma, respectively (Cosca et al., 1992; Busch and van der Pluijm, 1996; Busch et al., 1996). Regional structures of the Mazinaw domain are expressed as doubly plunging refolded isoclinal folds (Moore and Thompson, 1980; Ford, 1992), which are evident in outcrop patterns that show ENE-trending folds that close near the RLSZ (Fig. 1b).

The Sharbot Lake domain is lithologically distinct from the Mazinaw domain and is dominated by mafic and intermediate meta-igneous rock and marble (Fig. 1b). The most extensive plutonic complex, the Lavant gabbro, is chloritically altered and deformed along its western margin adjacent to the RLSZ. Marble is generally light blue and white, banded and coarse-grained in the central and eastern portions of the domain. Marbles are finer grained, darker colored and preserve bedding near the RLSZ. Metavolcanic rocks are veined (epidote, calcite) and include chloritically altered epidote-amphibolites with preserved primary volcanic features near the RLSZ (Easton, 1992). Away from the RLSZ, to the east, metavolcanic rocks are coarse crystalloblastic garnet–amphibole schists and gneisses. Based on preservation of primary structures, metamorphic textures and assemblages, the metamorphic grade increases to the south and east (Easton, 1988, 1992). This inference is supported by a single metamorphic isograd marking the transition from amphibolite to granulite facies assemblages in the southern Sharbot Lake domain (Fig. 1b, Carmichael et al., 1978).

Few radiometric ages have been reported from the Sharbot Lake domain. Wallach (1974) obtained a U/Pb zircon date of 1254 Ma for the Hinchinbrooke gneiss in the southern Sharbot Lake domain. A single U/Pb sphene date of 1152 Ma, interpreted as a metamorphic growth age, was obtained by Mezger et al. (1993). The Lavant gabbro has a U/Pb zircon age of 1225 Ma and sphene age of 1210 Ma (Corfu and Easton, 1994). Based on the lack of relatively young metamorphic ages (1000–1050 Ma) in the Sharbot Lake domain it has been concluded that the Sharbot Lake domain did not experience the younger metamorphism documented in the Mazinaw domain (Mezger et al., 1993; Corfu and Easton, 1994). Cooling ages ($^{40}Ar/^{39}Ar$) in the Sharbot Lake domain are much older (70–80 Ma) than those in the Mazinaw, which indicates the RLSZ was active until at least 900 Ma (Cosca et al., 1992; Busch and van der Pluijm, 1996; Busch et al., 1996).

3. Analytical techniques

Metamorphic mineral assemblages were characterized and appropriate samples were selected for thermobarometric determinations using polished thin sections and a standard petrographic microscope. A Cameca Camebax electron microprobe analyzer equipped with a backscattered electron imager at the University of Michigan was used to further characterize mineral assemblages and textures, and to determine mineral chemistries utilizing wavelength-dispersive analysis. Electron microprobe operating conditions were an accelerating voltage of 15 kV and a sample current of 10 nA except for micas, which were analyzed with a 12 kV accelerating voltage. A mixture of synthetic and natural mineral standards and correction routines of Pouchou and Pichoir (1984) (PAP) provided by Cameca were used. A point beam was used for all minerals except micas and feldspars, in which case the beam was rastered over a 9 μm^2 area to minimize loss of light elements.

The most abundant rock type suitable for thermobarometric determinations in the field area is garnet amphibolite (Fig. 2a). In these rocks, pressures were calculated using the empirically calibrated garnet–hornblende–plagioclase–quartz (GAPS) barometer of Kohn and Spear (1990). Peak metamorphic temperatures from garnet amphibolites were determined by the garnet–hornblende thermometer of Graham and Powell (1984), which is based on the partitioning of Fe and Mg between garnet and amphibole. Many garnet–amphibole and garnet–mica schists contain biotite (Fig. 2b). In these samples the garnet–biotite thermometer of Ferry and Spear (1978) with F corrections of Perchuk and Aranovich (1984) was used to estimate peak metamorphic temperatures. The garnet–aluminum silicate–quartz–plagioclase (GASP) barometer of Koziol and Newton (1988) was used to calculate pressure in one garnet–mica schist (Fig. 2c). Four garnet granulites were sampled in the field area (Fig. 2d). Peak metamorphic pressures were estimated using the pyroxene–garnet–plagioclase–quartz barometers of Moecher et al. (1988). In garnet granulites, tem-

Fig. 2. Backscattered electron images of (a) sample 137, garnet amphibole schist, (b) sample 60, garnet biotite schist, (c) sample 203, garnet granulite, and (d) sample 44, garnet mica schist. Scale bars are 500 μm. Abbreviations: g = garnet; p = plagioclase; q = quartz; h = hornblende; b = biotite; c = clinopyroxene; o = orthopyroxene; s = sillimanite; k = kyanite; st = staurolite; i = ilmenite; m = magnetite.

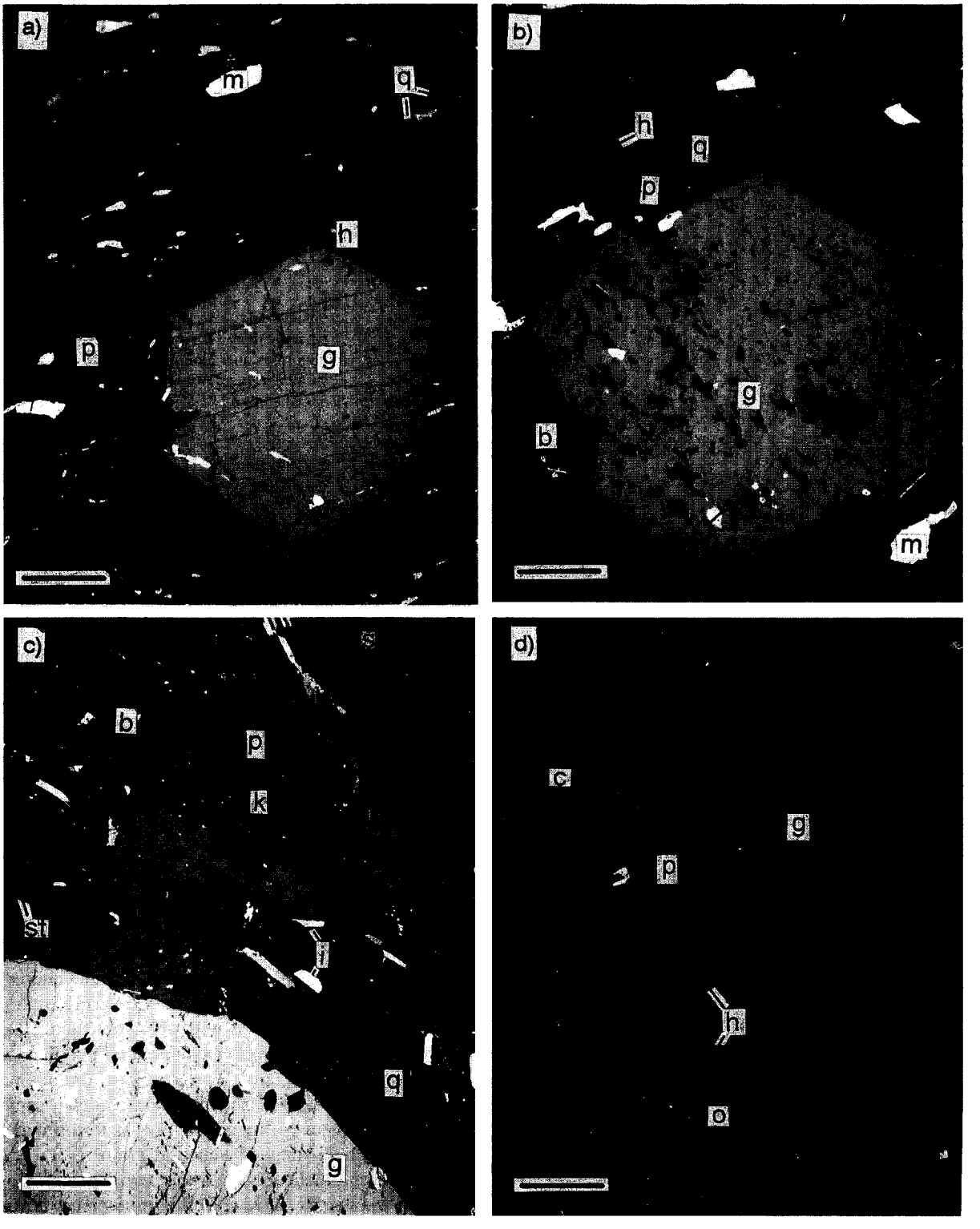
a)
m
q
h
p
g
b)
h
q
p
g
b
m
c)
b
p
k
si
l
q
g
d)
c
g
p
h
o

Table 1
Mineral assemblages in rocks used for thermobarometry

Sample	Garnet	Quartz	Plagioclase	Biotite	Hornblende	Other	Comment
35	X	X	X	X		zc, mt	
44	X	X	X	X		sil, ky, st, ru, trm, ilm, ap	relict ky
60	X	X	X	X	M	mt, ilm, zc, ap	
68	X	X	X	X	X	ap	
84	X	X	X	M	X	ilm, mt, ap	
137	X	X	X	M	X	mt, ilm, sphn, cc, ap	
140	X	X	X		X	cum, cc	
152	X	X	X	M	X	cum, ilm	
164	X	X	X	X	X	scp, cc	
170	X	X	X	X	X	zc	
173	X	M	X	X		opx	opx altered to fine white mica
179	X	X		X		ilm, ru, sphn, ap	pg completely sericitized
203	X	X	X		X	cpx, opx, mt, ap	minor cpx alteration to hb, corona textures
206	X	M	X	M	X	chl, ilm, mt, zc	chl replacement of bio, sericitized pg common
237	X	X	X		M	cpx, scp, cc, mt, ilm, py	cpx altered to hb
240	X	X	X		X	cum, ilm, ap	
242	X	X	X	X	M	py, zc, ap	
265	X	X	X		X	cpx, scp, sphn, cc, ap	cpx altered to hb
268	X	X	X		X	ilm	sericitized pg common
270	X	X	X	M	X	ap, mt, ilm	

X indicates major mineral phase. M indicates minor component. Abbreviations are: ap, apatite; cc, calcite; chl, chlorite; gt, garnet; ilm, ilmenite; ky, kyanite; mt, magnetite; opx, orthopyoxene; pg, plagioclase; py, pyrite; ru, rutile; scp, scpolite; sphn, sphene; st, staurolite; trm, tourmaline; zc, zircon.

peratures were calculated with the garnet–pyroxene Mg–Fe exchange thermometers of Ellis and Green (1979) and Harley (1984). Activity models from Elkins and Grove (1990) and Berman (1990) are used for plagioclase and garnet, respectively, in the application of GASP and garnet granulite barometers. Kohn and Spear (1990) used activity models of Hodges and Royden (1984) and Hodges and Spear (1982) in their empirical calibration; for comparison, results obtained using these activity models are also presented for GASP and the garnet granulite barometers (Table 1).

4. Petrography

Garnet–amphibole schist is the most abundant rock type selected for thermobarometry. These rocks contain the assemblage garnet–hornblende–plagioclase–quartz (Table 1). Samples that have chlorite or epidote replacement of hornblende or biotite were avoided. In general, garnet grains are small (1–3 mm), rounded, and subhedral with abundant inclusions (Fig. 2b). Inclusions in garnet are dominantly quartz. Hornblende grains are typically lath-shaped and subhedral to euhedral (Fig. 2a). Three samples also contain cummingtonite (Table 1). Plagioclase and quartz fill interstices between amphibole and garnet. Plagioclase is commonly twinned and shows optical zonation in some samples. Samples that have plagioclase with significant sericitic alteration were avoided.

Garnet–mica schists are used primarily for thermometry. These rocks contain the assemblage garnet–biotite–plagioclase–quartz (Table 1). Biotite grains are subhedral platelets (Fig. 2b). One mica schist was analyzed with the assemblage biotite–plagioclase–garnet–sillimanite–quartz–staurolite–muscovite–kyanite–ilmenite (Fig. 2c). Garnet grains are rounded with abundant inclusions of quartz, biotite, staurolite, kyanite, and plagioclase in the core of the grains. The matrix is dominated by biotite and plagioclase. Plagioclase shows some sericitic alteration. Sillimanite occurs as fibrolite and kyanite as small rounded anhedral grains (Fig. 2c). Both aluminum silicates are intergrown with plagioclase in the matrix. A few biotite grains have fibro-

lite intergrowths. The occurrence of anhedral kyanite and euhedral fibrolite is interpreted to represent the prograde transition from the kyanite to the sillimanite stability field, consistent with a clockwise *P–T* path.

A variety of garnet granulites are found in the study area. All samples contain textural evidence for an amphibolite facies overprint (Table 1). Pyroxenes commonly have overgrowths and intergrowths along cleavage planes of hornblende and fine cryptocrystalline material. Garnets are rounded and have jagged edges indicative of resorption. Garnets in sample 203 preserve coronal textures composed of plagioclase, hornblende, and orthopyroxene rinds, although these phases are not restricted to the coronas (Fig. 2d).

5. Mineral compositions

Garnet compositions are dominantly almandine (50–70%) with varied pyrope, grossular and spessartine components (Table 2). Garnet compositions were measured along traverses in each sample to assess the presence of compositional zoning. Compositional variation along garnet profiles are generally less than 5–10%. One typical characteristic is a decrease in pyrope content and an increase in almandine content in the outer 100–200 μm of garnet grains (Fig. 3). Most garnets show little zonation, but in cases where zonation was found the garnet composition that most nearly reflects the peak temperatures (highest Mg/[Mg + Fe]) was used. These compositions typically occur within 100–200 μm of the garnet rims (Fig. 3).

Traverses consisting of five spots were obtained in other minerals (hornblende, biotite, plagioclase, and pyroxene) used for thermobarometry. Grains adjacent to garnets and in the matrix several millimeters away from garnets were analyzed. In general, mineral compositions do not vary systematically with distance from garnet grains. Amphiboles generally have compositions between hornblende, tschermakite, and pargasite end-members ($1 < Al^{iv} < 2$, $1 < Al^{vi} + Fe^{3+} + Ti < 2$; Table 3). Systematic zonation in amphiboles was not detected in any samples; no compositional zonation was detected in biotite grains. Biotite compositions used for thermometry are reported in Table 4. Plagioclase compositions vary between samples from An_{20} to An_{50} with compositional zonation generally less than 5% (Table 5). Systematic compositional zonation ($\leq$20%) was detected in three samples. In these samples core compositions were used for thermobarometric determinations. Sample 203 has compositional zonation of An_{50} to An_{70} (core to rim) in plagioclase of the corona (Fig. 2d). Pyroxene grains are uniform in composition ($\leq$2% variation). Clinopyroxenes analyzed are 60–75% diopside (Table 6). Orthopyroxenes are intermediate in composition with approximately 50% ferrosilite (Table 6).

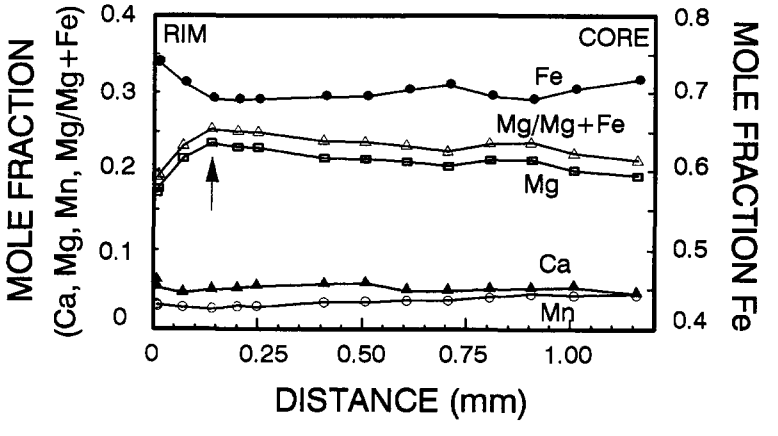

Fig. 3. A typical garnet compositional profile (sample 173). The profile is interpreted to represent prograde garnet growth (increasing Mg/[Mg + Fe]) with retrograde diffusional exchange characteristics near the rim. The arrow indicates the garnet composition used in thermobarometric determinations.

Table 2
Garnet compositions normalized to 12 oxygen atoms

Sample:	35	44	60	68	84	137	140	152	164	170	173	179	203	206	237	240	242	265	268	270
Wt% oxide																				
SiO_2	38.61	38.77	37.46	37.15	37.76	38.13	39.08	37.89	39.11	37.51	38.44	38.40	39.54	37.98	38.68	38.60	39.29	38.92	38.36	36.59
TiO_2	0.00	0.02	0.01	0.00	0.01	0.02	0.04	0.05	0.02	0.04	0.04	0.00	0.05	0.07	0.14	0.03	0.03	0.17	0.00	0.04
Al_2O_3	21.19	21.77	21.01	20.84	20.94	21.24	21.40	21.04	19.95	21.11	21.91	21.62	21.33	20.84	19.53	20.66	21.61	20.33	21.52	20.67
Cr_2O_3	0.00	0.01	0.05	0.00	0.04	0.04	0.01	0.01	0.00	0.12	0.03	0.02	0.06	0.00	0.02	0.00	0.02	0.00	0.04	0.00
FeO	29.94	30.09	28.69	30.78	29.74	28.63	29.00	30.66	24.27	34.13	31.92	30.97	24.42	30.94	23.82	31.24	25.53	23.11	26.89	32.21
MnO	6.09	2.62	5.02	3.21	3.60	5.44	1.57	2.81	2.24	1.32	1.24	1.11	1.31	2.93	2.01	2.80	0.74	3.89	2.29	1.82
MgO	4.56	4.79	2.99	1.55	3.06	4.18	5.48	2.58	1.50	3.14	5.94	4.39	6.61	3.21	1.48	2.41	4.65	1.02	6.62	1.77
CaO	1.05	2.92	4.51	5.50	4.44	2.88	4.46	5.39	12.97	2.46	1.91	4.48	6.69	4.07	14.23	4.63	8.63	12.78	3.77	6.14
Total	101.45	100.99	99.76	99.02	99.58	100.57	101.04	100.44	100.06	99.83	101.43	100.98	100.00	100.04	99.91	100.37	100.49	100.21	99.48	99.24
Number of ions																				
Si	3.033	3.027	3.003	3.016	3.024	3.015	3.034	3.017	3.091	3.010	2.989	3.007	3.051	3.030	3.070	3.071	3.042	3.075	3.006	2.977
Al	1.963	2.003	1.985	1.994	1.977	1.980	1.957	1.974	1.858	1.997	2.007	1.995	1.940	1.960	1.827	1.937	1.972	1.893	1.987	1.983
Ti	0.000	0.001	0.001	0.000	0.000	0.001	0.002	0.003	0.001	0.002	0.002	0.000	0.003	0.004	0.009	0.002	0.001	0.010	0.000	0.002
Cr	0.000	0.001	0.003	0.000	0.003	0.002	0.000	0.000	0.000	0.008	0.002	0.001	0.004	0.000	0.001	0.000	0.001	0.000	0.002	0.000
Mg	0.534	0.557	0.358	0.187	0.366	0.493	0.634	0.307	0.177	0.376	0.689	0.513	0.761	0.382	0.175	0.285	0.536	0.121	0.773	0.215
Fe	1.967	1.964	1.923	2.090	1.992	1.893	1.883	2.042	1.604	2.291	2.075	2.028	1.576	2.064	1.581	2.079	1.653	1.527	1.763	2.192
Mn	0.406	0.174	0.341	0.221	0.244	0.364	0.104	0.189	0.150	0.090	0.081	0.074	0.085	0.198	0.135	0.188	0.049	0.260	0.152	0.125
Ca	0.089	0.244	0.388	0.478	0.381	0.244	0.371	0.460	1.098	0.211	0.159	0.376	0.553	0.348	1.210	0.395	0.716	1.082	0.316	0.535
Mole%																				
Almandine	65.7	66.8	63.8	70.2	66.7	63.2	62.9	68.1	53.0	77.0	69.0	67.8	52.9	69.0	51.0	70.5	55.9	51.1	58.6	71.5
Grossular	3.0	8.3	12.9	16.1	12.8	8.1	12.4	15.3	36.3	7.1	5.3	12.6	18.6	11.6	39.0	13.4	24.2	36.2	10.5	17.4
Pyrope	17.8	18.9	11.9	6.3	12.3	16.5	21.2	10.2	5.8	12.6	22.9	17.1	25.5	12.8	5.6	9.7	18.1	4.0	25.7	7.0
Spessartine	13.6	5.9	11.3	7.4	8.2	12.2	3.5	6.3	5.0	3.0	2.7	2.5	2.9	6.6	4.4	6.4	1.7	8.7	5.1	4.1
Uvarovite	0.0	0.0	0.1	0.0	0.1	0.1	0.0	0.0	0.0	0.3	0.1	0.0	0.1	0.0	0.0	0.0	0.0	0.0	0.1	0.0
Mg#	0.214	0.221	0.157	0.082	0.155	0.207	0.252	0.131	0.099	0.141	0.249	0.202	0.326	0.156	0.100	0.121	0.245	0.073	0.305	0.089

Table 3
Hornblende compositions normalized to 13 small cations

Sample:	60	68	84	137	140	152	164	170	203	206	237	240	242	265	268	270
Wt% oxide																
SiO_2	44.04	41.77	42.34	42.44	45.06	43.96	44.93	42.70	39.90	41.27	42.37	41.96	44.20	41.75	44.66	40.74
Al_2O_3	11.92	12.01	12.90	14.71	13.63	11.09	10.59	14.92	13.77	13.83	10.61	10.64	11.82	10.77	15.17	12.36
TiO_2	0.60	0.98	0.81	0.42	0.69	0.89	0.78	0.65	2.01	0.57	1.14	1.34	0.85	0.97	0.70	0.69
Cr_2O_3	0.00	0.05	0.02	0.09	0.05	0.10	0.01	0.19	0.13	0.02	0.01	0.06	0.00	0.05	0.05	0.04
Fe_2O_3	8.40	7.25	9.94	10.92	7.96	6.19	4.16	6.02	1.91	6.92	5.67	7.31	5.92	3.68	5.79	11.33
FeO	11.55	18.09	11.70	7.63	6.63	14.05	14.98	12.93	14.08	11.63	16.48	15.97	11.00	21.55	6.90	12.61
MnO	0.46	0.29	0.38	0.41	0.13	0.12	0.19	0.10	0.15	0.40	0.09	0.31	0.09	0.16	0.18	0.22
MgO	8.52	5.01	7.51	8.74	11.26	8.49	9.03	7.68	9.81	8.45	7.51	6.53	9.95	4.91	11.51	6.53
CaO	10.90	10.87	10.43	10.17	11.05	11.14	11.87	11.08	11.82	11.00	11.64	10.73	11.01	11.59	11.16	10.04
Na_2O	1.28	1.40	1.88	1.78	1.37	1.49	1.12	1.37	1.81	2.08	1.61	1.75	1.26	1.63	1.68	2.15
K_2O	0.51	0.79	0.42	0.27	0.26	0.42	0.26	0.52	2.08	0.42	0.28	0.57	0.85	0.35	0.18	0.66
H_2O	2.15	2.12	2.15	2.25	2.34	2.18	2.23	2.07	1.92	2.09	2.23	2.22	2.17	2.17	2.36	1.94
F	0.24	0.15	0.20	0.12	0.00	0.10	0.10	0.20	0.56	0.01	0.00	0.00	0.24	0.04	0.00	0.00
Cl	0.00	0.02	0.01	0.00	0.07	0.11	0.00	0.35	0.08	0.61	0.02	0.02	0.02	0.02	0.04	0.96
O=F	−0.10	−0.07	−0.08	−0.05	0.00	−0.04	−0.04	−0.08	−0.24	0.00	0.00	0.00	−0.01	−0.02	0.00	0.00
O=Cl	0.00	0.00	0.00	0.00	−0.01	−0.02	0.00	−0.08	−0.02	−0.14	0.00	0.00	0.00	−0.01	−0.01	−0.22
Total	100.47	100.73	100.60	99.91	100.48	100.25	100.19	100.60	99.75	99.15	99.65	99.41	99.28	99.62	100.37	100.04
Number of ions																
T sites																
Si	6.487	6.344	6.266	6.201	6.448	6.539	6.669	6.292	6.045	6.201	6.435	6.409	6.539	6.474	6.383	6.175
Al^{iv}	1.513	1.656	1.734	1.799	1.552	1.461	1.331	1.708	1.955	1.799	1.565	1.591	1.461	1.526	1.617	1.825
M1, 2, 3, sites																
Al^{vi}	0.554	0.489	0.515	0.736	0.749	0.476	0.515	0.879	0.502	0.658	0.333	0.320	0.606	0.450	0.931	0.385
Ti	0.065	0.117	0.091	0.052	0.078	0.104	0.091	0.078	0.234	0.065	0.130	0.156	0.091	0.117	0.078	0.078
Fe^{3+}	0.931	0.830	1.107	1.198	0.855	0.694	0.465	0.665	0.218	0.781	0.650	0.841	0.659	0.430	0.619	1.290
Fe^{2+}	1.526	2.394	1.571	1.064	0.887	1.828	1.914	1.662	1.810	1.546	2.171	2.136	1.434	2.846	0.889	1.739
Mn	0.052	0.039	0.052	0.052	0.013	0.013	0.026	0.013	0.013	0.052	0.013	0.039	0.013	0.026	0.026	0.026
Mg	1.872	1.131	1.664	1.898	2.405	1.885	2.002	1.690	2.210	1.898	1.703	1.482	2.197	1.131	2.457	1.469
Cr	0.000	0.000	0.000	0.013	0.000	0.013	0.000	0.026	0.013	0.000	0.000	0.013	0.000	0.000	0.000	0.000
M4 site																
Ca	1.718	1.769	1.655	1.590	1.695	1.775	1.886	1.747	1.918	1.772	1.896	1.758	1.746	1.926	1.707	1.631
Na	0.282	0.231	0.345	0.410	0.305	0.225	0.114	0.253	0.082	0.228	0.104	0.242	0.254	0.074	0.293	0.369
A site																
Na	0.084	0.182	0.196	0.094	0.077	0.203	0.209	0.138	0.448	0.378	0.372	0.274	0.108	0.416	0.171	0.262
K	0.096	0.152	0.079	0.051	0.046	0.079	0.048	0.097	0.401	0.080	0.054	0.112	0.160	0.070	0.033	0.127
Anion sites																
O	22.000	22.000	22.000	22.000	22.000	22.000	22.000	22.000	22.000	22.000	22.000	22.000	22.000	22.000	22.000	22.000
OH	1.888	1.920	1.905	1.945	1.985	1.926	1.953	1.819	1.711	1.842	1.995	1.995	1.881	1.975	1.991	1.752
F	0.111	0.075	0.093	0.055	0.000	0.047	0.047	0.094	0.269	0.003	0.000	0.000	0.115	0.018	0.000	0.000
Cl	0.001	0.005	0.002	0.000	0.015	0.027	0.000	0.087	0.020	0.155	0.005	0.005	0.004	0.007	0.009	0.248

6. Thermobarometric results

A total of 31 samples were analyzed for thermobarometry, which resulted in 13 pressures and 18 temperatures due to compositional limits of thermobarometric calibrations. Errors in thermobarometry were estimated by combining the standard error in thermobarometric calibrations, error in temperature used for barometry, the statistical error in electron microprobe analysis, and errors from sample heterogeneity (grain to grain compositional differences). The resulting errors are typically <40°C and ±100 MPa (1σ). Errors in pressure and temperature differences between samples (differential errors) relate to the compositional uncertainties arising from analytical precision and sample heterogeneity (Hodges and McKenna, 1987; Kohn and Spear, 1991). Pressures calculated in this paper are predominantly from one barometer so differential errors will be used for GAPS. Differential errors were estimated by combining electron microprobe analytical error, pressure error due to uncertainty in temperature, and the standard deviation of pressures obtained using different hornblende compositions. Differential errors are 30–60 MPa (1σ) with typically 50% of the error arising from analytical error, 20% from the error in temperature, and 30% from sample heterogeneity. An absolute error of 50°C is used for thermometry. Pressures obtained from GASP and granulite assemblages are not assigned errors and are presented for comparison with GAPS pressures.

Peak metamorphic temperatures and pressures calculated are listed in Table 7. In general, there is good agreement between the thermobarometers.

Table 4
Biotite compositions normalized to 14 small cations

Sample:	35	44	170	173	179
Wt% oxide					
SiO_2	35.74	36.67	35.69	35.57	36.42
TiO_2	2.76	2.09	1.45	3.18	1.48
Al_2O_3	16.53	19.02	16.76	16.16	17.18
Cr_2O_3	0.12	0.05	0.14	0.10	0.00
FeO	17.92	16.83	20.57	19.91	18.09
MnO	0.21	0.02	0.02	0.01	0.08
MgO	12.13	12.13	11.89	10.80	12.89
BaO	0.00	0.27	0.19	0.50	0.05
CaO	0.00	0.00	0.05	0.03	0.02
Na_2O	0.10	0.25	0.12	0.07	0.30
K_2O	9.49	8.95	8.62	9.61	9.02
F	0.32	0.41	0.13	0.00	0.41
Cl	0.00	0.00	0.41	0.27	0.50
H_2O	3.14	3.04	3.72	3.00	3.31
O=F	−0.13	−0.17	−0.05	−0.00	−0.17
O=Cl	−0.00	−0.00	−0.09	−0.06	−0.11
Total	98.32	99.56	99.60	99.16	99.46
Number of ions					
Si	5.521	5.529	5.456	5.542	5.531
Aliv	2.479	2.471	2.544	2.458	2.469
Alvi	0.530	0.909	0.476	0.510	0.606
Ti	0.320	0.237	0.166	0.373	0.169
Cr	0.015	0.005	0.016	0.012	0.000
Fe	2.315	2.122	2.630	2.595	2.298
Mn	0.027	0.002	0.003	0.001	0.010
Mg	2.792	2.725	2.709	2.509	2.918
Ba	0.000	0.016	0.012	0.031	0.003
Ca	0.000	0.000	0.008	0.006	0.003
Na	0.029	0.074	0.034	0.020	0.089
K	1.871	1.721	1.682	1.911	1.747
A site	1.900	1.795	1.716	1.931	1.835
O	20.000	20.000	20.000	20.000	20.000
O (OH site)	0.607	0.744	0.036	0.814	0.322
F	0.154	0.194	0.061	0.000	0.199
Cl	0.000	0.000	0.106	0.072	0.130
OH	3.239	3.061	3.797	3.115	3.349

The data, including those from Rathmell (1993) and Cureton (1994) in the south-central Mazinaw domain, are shown in map form in Fig. 4. At several locations results obtained with different barometers can be compared. Proximal samples (140 and 44, 173 and 170; Table 6) yield similar pressures, which lends confidence to the accuracy of the barometry. The temperature data from various thermometers are generally consistent. However, in the central Sharbot Lake and southeast Mazinaw domains results that differ by up to 200°C were obtained (Fig. 4b).

The data show regional differences in metamorphic grade and peak metamorphic pressure across the study area (Fig. 4). Peak values are discontinuous in the vicinity of the RLSZ. Peak metamorphic pressure is 800 MPa in the footwall and 500 MPa in rocks directly across the RLSZ in the hanging wall. Moreover, the metamorphic field gradient varies systematically on either side of the zone (Fig. 4). Pressure gradients are defined by six points in the south-central portion of the field area where data on either side of the zone can be directly compared (Fig. 4a). Data projected parallel to the strike of the shear zone also lie along these gradients, suggesting consistency in the gradients from north to south (Fig. 5). A sharp increase in pressure from 550 MPa to 800 MPa occurs within 8 km of the RLSZ in the footwall (Fig. 5b). In the hanging wall pressures increase away from the RLSZ from 500 MPa to 900 MPa within 12 km of the RLSZ (Fig. 5b).

7. Discussion

The baric field gradient is well defined and consistent from north to south (Fig. 5); the thermometric field gradient is less well defined. Temperature variations vaguely follow pressure variations across the field area, but the gradient in peak metamorphic temperature across the region is less well defined and there are areas where results are not consistent. The lack of consistency and definition in the thermometric field gradient is attributed primarily to the resetting of thermometers during cooling. Complex geothermal structure associated with thermotectonic metamorphism and local thermal perturbations caused by magmatism may also play a role (e.g. sample 173 is located within 1 km of a mafic intrusive). However, barometers are only slightly sensitive to temperature and because they generally involve mineral structural changes, as opposed to cation exchange, they are not reset as easily.

The existing geochronologic data (Mezger et al., 1993; Corfu and Easton, 1994) and contrast in peak metamorphic conditions inferred from thermobarometry suggest that the Mazinaw and Sharbot Lake domains are distinct in terms of metamorphic history. The metamorphic facies and thermobarometry indicate upper greenschist to lower amphibolite facies metamorphic conditions in most of the Mazinaw do-

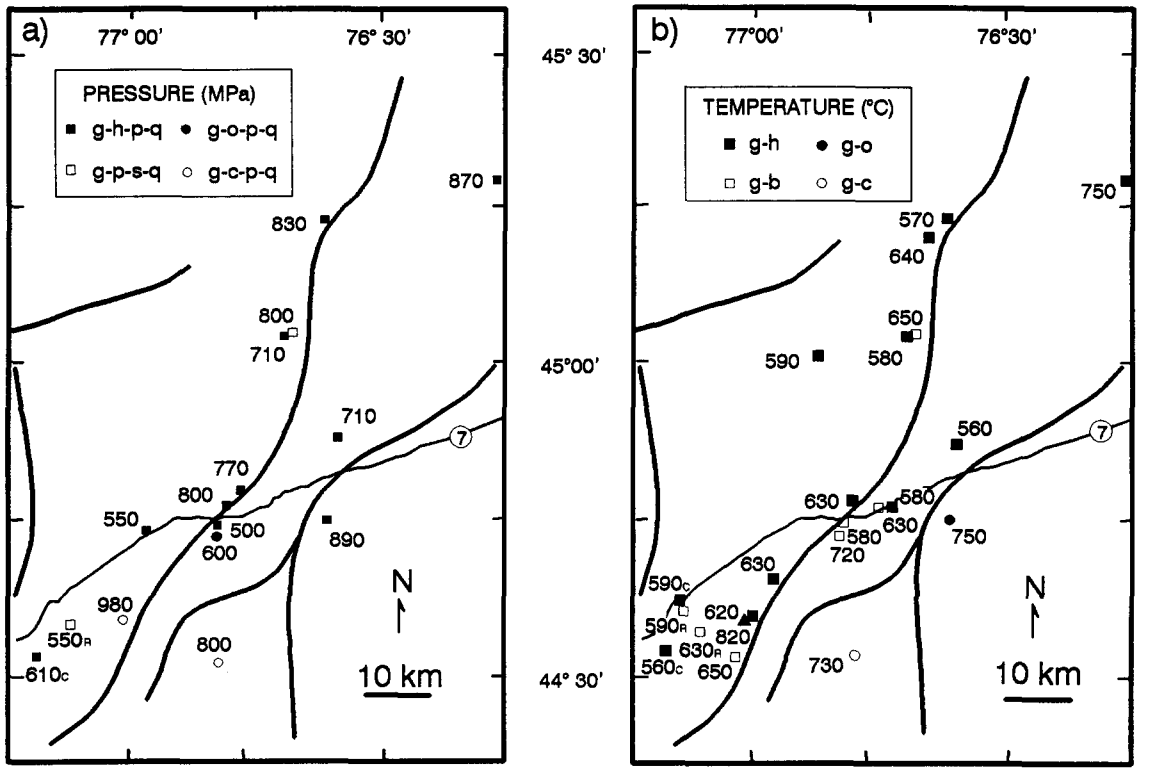

Fig. 4. Maps of the study area with (a) peak metamorphic pressures and (b) peak metamorphic temperatures. Abbreviations are the same as in Fig. 2. Subscript C indicates values calculated from data of Cureton (1994) and subscript R indicates value from Rathmell (1993).

Table 5
Plagioclase compositions normalized to 8 oxygen atoms

Sample:	44	60	84	137	140	152	170	173	203	206	237	242	265
Wt% oxide													
SiO_2	59.09	61.75	61.99	60.09	59.59	62.40	60.46	58.78	54.04	60.10	54.46	55.48	59.81
Al_2O_3	25.88	24.04	24.07	25.17	25.53	23.38	25.11	26.16	28.51	25.16	28.54	27.77	25.17
Fe_2O_3	0.18	0.26	0.04	0.03	0.05	0.07	0.04	0.09	0.06	0.05	0.06	0.12	0.03
CaO	7.72	5.07	5.38	6.89	7.36	4.78	6.57	8.06	10.79	6.29	10.60	9.81	6.54
Na_2O	7.09	8.84	8.59	7.79	7.65	9.04	8.17	6.98	5.44	8.05	5.62	5.91	7.98
K_2O	0.44	0.04	0.07	0.04	0.04	0.04	0.03	0.08	0.23	0.04	0.05	0.12	0.06
Total	100.40	100.00	100.14	100.00	100.22	99.70	100.38	100.15	99.07	99.69	99.33	99.20	99.59
Number of ions													
Si	2.633	2.740	2.744	2.676	2.653	2.772	2.682	2.622	2.463	2.681	2.472	2.515	2.674
Al	1.359	1.257	1.256	1.321	1.340	1.224	1.313	1.375	1.531	1.323	1.527	1.483	1.326
Fe^{+3}	0.006	0.009	0.001	0.001	0.002	0.002	0.001	0.003	0.002	0.002	0.002	0.004	0.001
Ca	0.368	0.241	0.255	0.329	0.351	0.227	0.312	0.385	0.527	0.301	0.516	0.476	0.313
Na	0.612	0.761	0.737	0.673	0.660	0.778	0.702	0.604	0.481	0.697	0.495	0.519	0.691
K	0.025	0.002	0.004	0.002	0.002	0.002	0.002	0.005	0.013	0.002	0.003	0.007	0.003
mole%													
Anorthite	36.6	24.0	25.6	32.7	34.6	22.6	30.7	38.8	51.6	30.1	50.9	47.5	31.1
Albite	60.9	75.8	74.0	67.0	65.2	77.2	69.1	60.8	47.1	69.7	48.8	51.8	68.6
Orthoclase	2.5	0.2	0.4	0.2	0.2	0.2	0.2	0.5	1.3	0.2	0.3	0.7	0.3

Table 6
Pyroxene compositions normalized to 4 cations and 6 oxygen atoms

Sample:	173 opx	203 opx	203 cpx	237 cpx	265 cpx
Wt% oxide					
SiO_2	48.84	50.51	50.09	48.94	49.46
TiO_2	0.12	0.01	0.28	0.48	0.12
Al_2O_3	1.34	1.53	4.56	3.64	1.22
Fe_2O_3	0.00	0.00	0.00	0.00	0.00
Cr_2O_3	0.00	0.00	0.00	0.06	0.00
FeO	32.95	28.25	10.33	14.87	20.51
MnO	1.61	0.95	0.41	0.65	0.39
MgO	14.73	18.70	11.71	8.82	6.10
CaO	0.42	0.92	21.75	21.83	21.64
Na_2O	0.02	0.01	0.67	0.65	0.43
Total	100.05	100.88	99.82	99.94	99.88
Number of ions					
Si	1.922	1.915	1.878	1.876	1.949
Al^{iv}	0.062	0.069	0.122	0.124	0.051
Al^{vi}	0.000	0.000	0.080	0.041	0.005
Ti	0.004	0.000	0.008	0.014	0.004
Fe^{3+}	0.066	0.076	0.056	0.077	0.055
Cr	0.000	0.000	0.000	0.002	0.000
Mg	0.864	1.057	0.655	0.504	0.358
Fe	1.018	0.820	0.268	0.400	0.621
Mn	0.044	0.025	0.011	0.017	0.011
Ca	0.018	0.037	0.874	0.897	0.913
Na	0.002	0.001	0.049	0.049	0.033

main. The Sharbot Lake domain is characterized by upper amphibolite to granulate facies metamorphic conditions. The divergence from this characterization occurs adjacent to the RLSZ, where thermobarometric results indicative of upper amphibolite facies and upper greenschist facies occur in the Mazinaw and Sharbot Lake domains, respectively.

The variation in peak metamorphic pressure across the region near the RLSZ yields important clues to the style of extension if constraints are placed on the initial barometric structure of the crust. The steep gradients in metamorphic pressure only occur adjacent to the RLSZ, which suggests that the variation is due to deformation along the zone. If the steep gradients in pressure existed without offset before displacement on the RLSZ, the offset in pressure could be used to calculate the displacement of the shear zone (Fig. 6). However, because the age of metamorphism is different on either side of the RLSZ, continuity in isobaric surfaces across the zone is not likely. Could compression (thrusting or folding) have produced the observed variation in metamorphic pressure? To generate folded isobaric surfaces requires a 20 km wide zone of distributed shear or folding during compression (Fig. 6). The difference in metamorphic age between the two domains then requires that the Sharbot Lake domain was not metamorphosed as it was thrust over the Mazinaw domain during the 995–1050 Ma tectonometamorphic event and deformation in the vicinity of the RLSZ was not accompanied by metamorphism, which would reset the mineral equilibrium compositions and erase the pre-thrusting isobars. This scenario is considered unlikely because: (1) there is no field evidence for a thrust history, and (2) extension occurred at mid-crustal levels and thus, this hypothetical compression would be deep-seated and involve prograde metamorphism, resetting the thermobarometric systems in the footwall.

The favored interpretation assumes initially horizontal isobars in two adjacent domains in the Metasedimentary Belt. The assumption of horizontal isobars is valid if the pressures used to define isobars within each domain are recording the same metamorphism in each domain. The existing chronologic data do not indicate synchronous metamorphism between the domains, but the ages within each domain are consistent with the assumption of horizontal isobars. Although Corfu and Easton (1995) find differences in metamorphic age between structural domains within the northern Mazinaw domain, the samples used to obtain metamorphic data in the south-central portion of the study area (Fig. 4, along near highway 7) lie within the same structural domain and therefore likely have uniform metamorphic ages. Furthermore, the baric field gradient defined by samples from other portions of the domain (when projected along strike) is consistent with the baric gradient defined by samples within the structural domain in the south-central portion of the study area. The age of metamorphism in the Sharbot Lake domain is constrained by only one age (1152 Ma, Mezger et al., 1993), so uniformity in metamorphic age within the Sharbot Lake domain cannot be tested with presently available data.

Prior to extension the Sharbot Lake domain is juxtaposed with the Mazinaw domain (Fig. 7a). The difference in age of metamorphism between the Mazinaw and Sharbot Lake domains has been

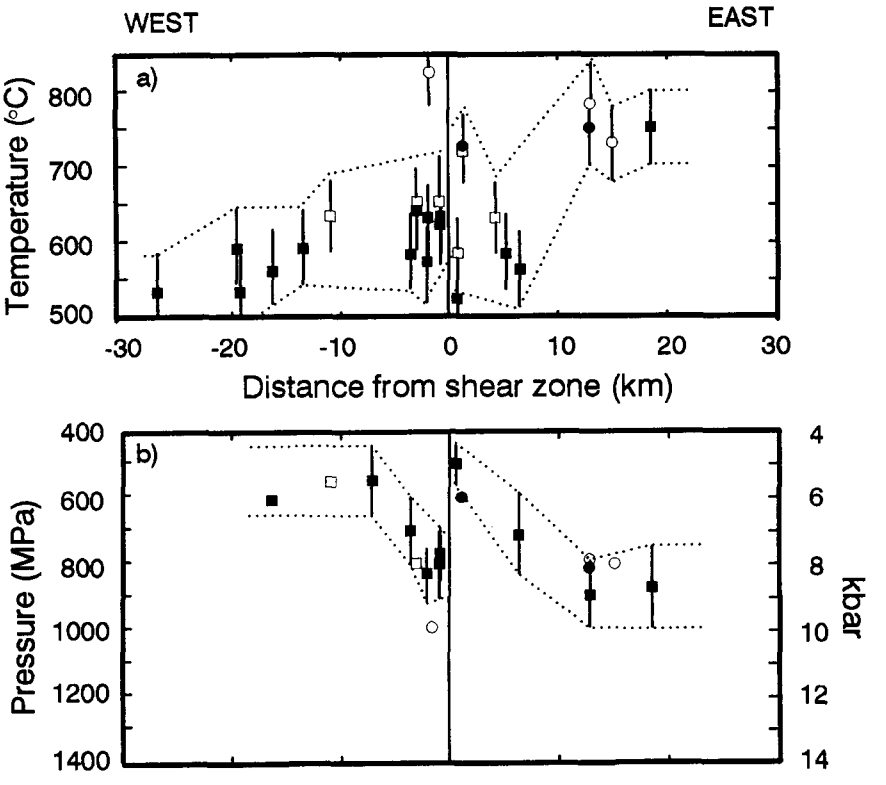

Fig. 5. Peak metamorphic temperatures (a) and pressures (b) versus distance from the RLSZ. Distance is measured perpendicular to the strike of the shear zone. Error bars are ±50°C in (a) and differential errors (±60–120 Mpa, 2σ) for pressure using the barometer of Kohn and Spear (1990) in (b). All data from Fig. 4 plus values outside the study area from Rathmell (1993) are included. Symbols correspond to thermobarometers as in Fig. 4.

used to suggest that the RLSZ was the site of an ancient suture (Mezger et al., 1993), which is supported by differences in metamorphic pressure and temperature. Extension is initiated along this high-angle major crustal discontinuity. Displacement along the RLSZ and associated unroofing leads to isostatic adjustments of footwall uplift and hanging-wall subsidence (Spencer, 1984; Buck, 1988; Wernicke and Axen, 1988; Kusznir et al., 1991). Isostatic response to fault motion rotates the pre-existing isobaric surfaces via crustal flexure (Fig. 7), which is localized near the RLSZ in a zone 20 km wide at the present erosional level. Because the pre-extensional history of the Grenville Orogen is complex and polycyclic, field evidence for the model is difficult to ascertain. However, geometric consequences of the model that are consistent with field evidence are the presence of fold closures (Fig. 1) and shallowing of structural elements near the RLSZ (Busch and van der Pluijm, 1996). In addition, thermochronologic data are consistent with this model and indicate uniform unroofing of the footwall since ~950 Ma and differential unroofing of the hanging wall since 1029 Ma (Busch et al., 1996), requiring that the isostatic flexural rotations occurred between 1029 Ma and 950 Ma.

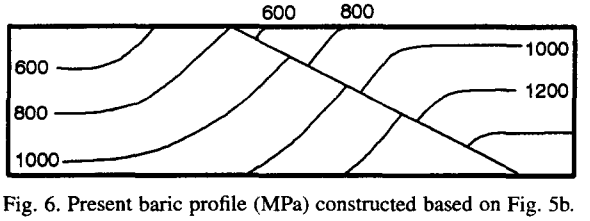

Fig. 6. Present baric profile (MPa) constructed based on Fig. 5b.

This model requires that the RLSZ rotated from a high dip angle during extension. The magnitude

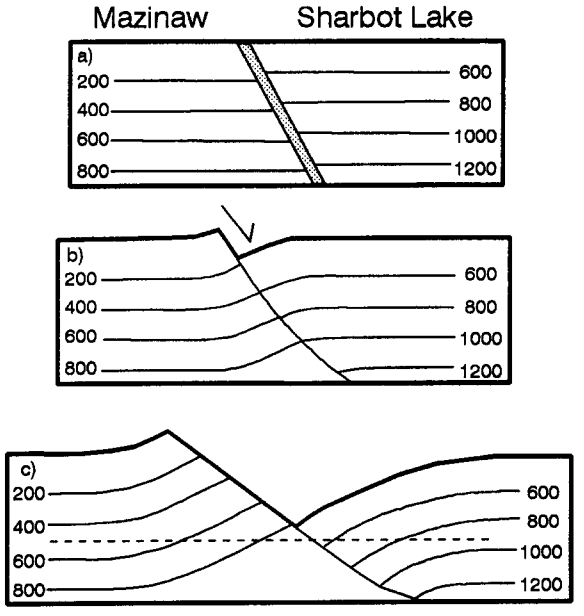

Fig. 7. Geometric model. (a) Pre-extension crustal baric profile (MPa) with the Mazinaw–Sharbot Lake suture stippled. (b) Initiation of extension and isostatic flexural rotations. (c) Further rotation associated with displacement. Dotted line represents the present erosional level. The model reproduces the baric field gradient.

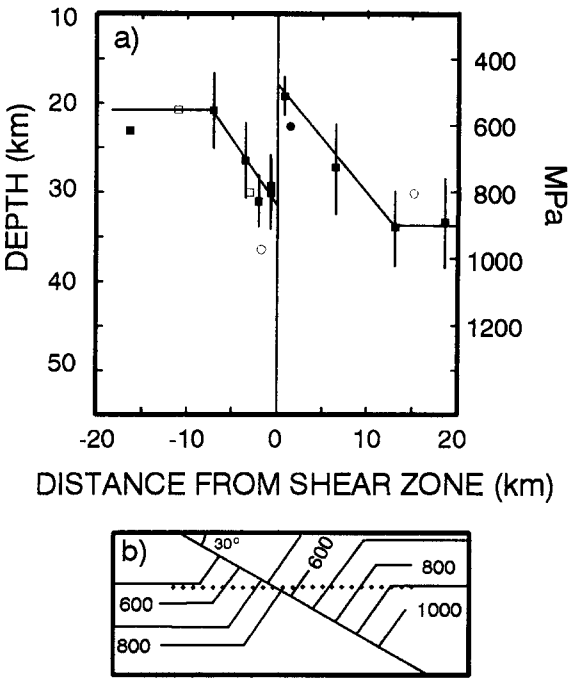

Fig. 8. (a) Depth calculated from metamorphic pressure versus distance from the RLSZ. Symbols are the same as in Fig. 4a. (b) Scaled geometric model illustrating rotated isobars (MPa) to produce the paleodepth versus distance variation in (a). The degree of hinge migration is greater in the hanging wall. The dotted line is the present erosional level.

of rotation can be estimated from the barometric data, and estimates of the magnitude of rotation derived independently from data in the hanging wall and footwall should be compatible. For simplicity the baric gradients are approximated with line segments (Fig. 8a). Depths associated with pressure estimates are calculated using a crustal density of 2700 kg/m^3. The baric gradients near the RLSZ are determined by the degree of rotation, and yield rotation angles of 50°and 60° for the hanging wall and footwall, respectively. Given the present orientation of the RLSZ (~30°), a steep initial dip (65°–90°) of the Mazinaw–Sharbot Lake domain boundary is obtained. Due to errors associated with barometry the precise pre-extension orientation cannot be determined and the detailed geometry of flexure cannot be resolved. However, a major crustal flexure of the deep crust would likely include ductile flow and a smoothly curved flexure is therefore preferred.

Existing models of isostatically induced crustal flexure incorporate a decoupling horizon at 15–20 km depth (Buck, 1988; Wernicke and Axen, 1988; Kusznir et al., 1991), which is not supported by the present data in the Grenville Orogen. Recent seismic studies show a set of reflectors correlating with the Mazinaw–Sharbot Lake terrane boundary (RLSZ) that dip ~13° from 8 to 24 km depth (White et al., 1994; Zelt et al., 1994). Given that exposures of the RLSZ indicate displacement at depths associated with the plastic to brittle transition (15 km) (Busch and van der Pluijm, 1996), an original depth extent of at least 40 km is inferred from these combined data. Thus, if a decoupling horizon existed and regional-scale plastic flow accommodated extension, it must have occurred below ~40 km depth, which is well into the crystal–plastic deformation regime of crustal rocks. Adding the depth at which the zone was active (at least 15 km) to the present 45 km crustal thickness (Zelt et al., 1994), yields a crustal thickness of 60 km during extension, assuming no addition of material to the base of the crust since extension. Therefore, if regional-scale plastic flow accommodated flexure it must have occurred

Table 7
Peak metamorphic pressures and temperatures with Universal Transverse Mercator grid coordinates of sample locations

Sample	Temperature (°C)				Pressure (MPa)				UTM coordinates	
	1	2	3	4	5	6	7	8	Northing	Easting
35	650								4932090	338550
44	650							800(810)	4989310	366860
60					770				4961475	358895
68		630							4947050	344320
84		630			800				4959455	357290
137					550				4955575	344760
140		580			710				4989250	366210
152		570			830				5010675	372390
164		640							5003920	370350
170	580	520			500				4955620	354610
173	720		720			600(570)			4954610	354630
179	630								4959180	363370
203			750	780	890	820(800) [a]	780(670)		4757460	372380
206		560			710				4970875	372890
237				730			800(700)		4932900	356370
240		620							4939150	341420
242		750			870				5015650	398910
265				820			980(900)		4937950	339070
268		590							4984770	449910
270		580							4958900	364140

1, garnet–biotite; 2, garnet–hornblende; 3, garnet–orthopyroxene; 4, garnet–clinopyroxene; 5, garnet–amphibole–plagioclase; 6, garnet–plagioclase–ferrosilite–quartz; 7, garnet–plagioclase–diopside–quartz; 8, garnet aluminum silicate–quartz–plagioclase. Pressures in parentheses are determined using activity models of Hodges and Royden (1984) and Hodges and Spear (1982) for comparison.
[a] Calculated with plagioclase composition in corona (An_{72}).

in the lower third of the crust (Fig. 9). A modified version of the flexural models of Buck (1988) and Kusznir et al. (1991) with a decoupling horizon just above the crust–mantle boundary may apply. Perhaps the decoupling horizon correlates with the detachment horizon inferred for thrust faults west of the study area (White et al., 1994), which is the mid-crustal discontinuity imaged by Zelt et al. (1994) currently at 30 km depth. Alternatively, the RLSZ may have cut deeper into the lithosphere and decoupling occurred at the Moho or in the upper mantle, with extension accommodated by asthenospheric regional-scale flow (Wernicke, 1981). Presently, the crust–mantle boundary is relatively flat and therefore such a deep-seated detachment is unlikely.

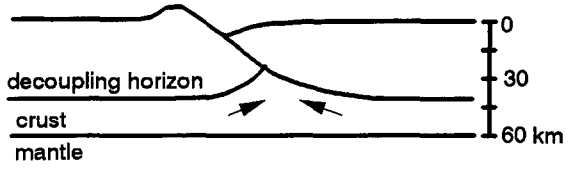

Fig. 9. Schematic diagram illustrating the flexural rotation of the crustal slab with regional plastic flow accommodating extension in the lower 1/3 (20 km) of the crust below the decoupling horizon (~40 km depth). The diagram is constrained by the depth of displacement based on low-temperature mylonites and plastic to brittle structures (15 km, Busch and van der Pluijm, 1996), and the present depth extent of the RLSZ (25 km) and present crustal thickness (45 km) from seismic observations (Zelt et al., 1994).

Acknowledgements

Grants from the National Science Foundation (EAR 93-05736), the Scott Turner Fund (at the University of Michigan), and Geological Society of America (4875-92 and 5122-93) provided financial support for this project. The electron microprobe analyzer used in this work was acquired under Grant EAR 82-12764 from the National Science Foundation. We are grateful for reviews by K.V. Hodges and J.M. McLelland.

References

Andersen, T.B. and Jamtveit, B., 1990. Uplift of deep crust during orogenic extensional collapse: a model based on field studies in the Sogn–Sunnfjord region of western Norway. Tectonics, 9: 1097–1111.

Anovitz, L.M. and Essene, E.J., 1990. Thermobarometry and pressure–temperature paths in the Grenville Province of Ontario. J. Petrol., 31: 197–241.

Barr, D., 1987. Lithospheric stretching, detached normal faulting and footwall uplift. In: M.P. Coward, J.F. Dewey and P.L. Hancock (Editors), Continental Extensional Tectonics. Geol. Soc. London Spec. Publ., 28: 75–94.

Berman, R.G., 1990. Mixing properties of Ca–Mg–Fe–Mn garnets. Am. Mineral., 75: 328–344.

Block, L. and Royden, L.H., 1990. Core complex geometries and regional scale flow in the lower crust. Tectonics, 9: 557–567.

Brodie, K.H. and Rutter, E.H., 1987. Deep crustal extensional faulting in the Ivrea zone of northern Italy. Tectonophysics, 140: 193–212.

Brun, J.-P. and Choukroune, P., 1983. Normal faulting, block tilting, and decollement in a stretched crust. Tectonics, 2: 345–356.

Buck, W.R., 1988. Flexural rotation of normal faults. Tectonics, 7: 959–973.

Busch, J.P. and van der Pluijm, B.A., 1996. Late orogenic, plastic to brittle extension along the Robertson Lake shear zone: implications for the style of deep-orogenic extension in the Grenville orogen, Canada. Precambrian Res., 77: 41–58.

Busch, J.P., van der Pluijm, B.A., Hall, C.M. and Essene, E.J., 1996. Listric normal faulting during post-orogenic extension revealed by $^{40}Ar/^{39}Ar$ thermochronology near the Robertson Lake shear zone, Grenville orogen, Canada. Tectonics, 15: 387–402.

Carlson, K.A., van der Pluijm, B.A. and Hanmer, S., 1990. Marble mylonites of the Bancroft shear zone: evidence for extension in the Canadian Grenville. Geol. Soc. Am. Bull., 102: 174–181.

Carmichael, D.M., Moore, J.M. and Skippen, G.B., 1978. Isograds around the Hastings metamorphic 'low'. Geol. Soc. Am. – Geol. Assoc. Can. – Mineral. Assoc. Can., Toronto 1978, Field Trip Guidebook, pp. 325–346.

Corfu, F. and Easton, R.M., 1994. U/Pb geochronology of the Mazinaw terrane, Central Metasedimentary Belt, Grenville Province, Ontario. Prog. Abstr., Geol. Assoc. Can. – Mineral. Assoc. Can., 19: A22.

Corfu, F. and Easton, R.M., 1995. U/Pb geochronology of the Mazinaw terrane, an imbricate segment of the Central Metasedimentary Belt, Grenville Province, Ontario. Can. J. Earth Sci., 32: 959–976.

Cosca, M.A., Essene, E.J., Kunk, M.J. and Sutter, J.F., 1992. Differential unroofing within the Central Metasedimentary Belt of the Grenville Orogen: constraints from $^{40}Ar/^{39}Ar$ thermochronology. Contrib. Mineral. Petrol., 110: 211–225.

Culshaw, N.G., Ketchum, J.W.F., Wodicka, N. and Wallace, P., 1994. Deep crustal extension following thrusting in the southwestern Grenville Province, Ontario. Can. J. Earth. Sci., 31: 160–175.

Cureton, J.S., 1994. Late orogenic normal faulting along the Mooroton shear zone, Grenville Province, Ontario, Canada. M.Sc. Thesis, Univ. of Michigan, Ann Arbor.

Davidson, A., 1984. Tectonic boundaries within the Grenville Province of the Canadian shield. J. Geodyn., 1: 433–444.

Davidson, I., 1989. Extensional domino fault tectonics: kinematics and geometrical constraints. Ann. Tectonicae, III: 12–24.

Davis, G.H., 1983. Shear-zone model for the origin of metamorphic core complexes. Geology, 11: 342–347.

Dunn, S.R. and Gilliam, C.E., 1994. Garnet zoning and interpretation of the pressure–temperature history for a portion of the Elzevir terrane, Grenville Province, S. Ontario. Geol. Soc. Am. Abstr. Prog., 26: A225.

Easton, R.M., 1988. Regional mapping and stratigraphic studies, Grenville Province with some notes on mineralization environments. In: A.C. Colvine, M.E. Cherry, B.O. Dressler, P.C. Thruston, C.L. Baker, R.B. Barlow and C. Riddle (Editors), Summary of Field Work and Other Activities. Ont. Geol. Surv., Misc. Pap., 141: 300–308.

Easton, R.M., 1992. Part 2, The Grenville Province and the Proterozoic history of central and southern Ontario. In: P.C. Thurston, H.R. Williams, R.H. Sutcliffe and G.M. Stott (Editors), Geology of Ontario. Ont. Geol. Surv. Spec. Vol., 4: 714–904.

Elkins, L.T. and Grove, T.L., 1990. Ternary feldspar experiments and thermodynamic models. Am. Mineral., 75: 544–559.

Ellis, D.J. and Green, D.H., 1979. An experimental study of the effect of Ca upon garnet–clinopyroxene Fe–Mg exchange equilibria. Contrib. Mineral. Petrol., 71: 13–22.

Ferry, J.M. and Spear, F.S., 1978. Experimental calibration of the partitioning of Fe and Mg between biotite and garnet. Contrib. Mineral. Petrol., 66: 113–117.

Ford, F., 1992. Geology of the Fernleigh and Ompah 'synclines', Palmerston Lake area. Ont. Geol. Surv. Misc. Pap., 160: 41–46.

Gans, P.B., 1987. An open-system, two-layer crustal stretching model for the eastern Great Basin. Tectonics, 6: 1–12.

Gans, P.B., Miller, E.L., McCarthy, J. and Ouldcott, M.L., 1985. Tertiary extensional faulting and evolving ductile–brittle transition zones in the northern Snake Range and vicinity: new insights from seismic data. Geology, 13: 189–193.

Graham, C.M. and Powell, R., 1984. A garnet–hornblende geothermometer, calibration, testing, and application to the Pelona Schist, Southern California. J. Metamorph. Geol., 2: 13–31.

Hanmer, S., 1988. Ductile thrusting at mid-crustal levels, southwestern Grenville Province. Can. J. Earth Sci., 25: 1049–1059.

Harley, S.L., 1984. An experimental study of the partitioning of Fe and Mg between garnet and orthopyroxene. Contrib. Mineral. Petrol., 86: 359–373.

Hodges, K.V. and Spear, F.S., 1982. Geothermometry, geobarometry and the Al_2SiO_5 triple point at Mt. Moosiliauke, New Hampshire. Am. Mineral., 67: 1118–1134.

Hodges, K.V. and Royden, L., 1984. Geologic thermobarometry of retrograded metamorphic rocks: an indication of the uplift trajectory of a portion of the northern Scandinavian

Caledonides. J. Geophys. Res., 89: 7077–7090.
Hodges, K.V. and McKenna, L.W., 1987. Realistic propagation of uncertainties in geologic thermobarometry. Am. Mineral., 72: 671–680.
Hodges, K.V., Burchfiel, B.C., Royden, L.H., Chen, Z. and Liu, Y., 1993. The metamorphic signature of contemporaneous extension and shortening in the central Himalayan orogen: data from the Nyalam transect, southern Tibet. J. Metamorph. Geol., 11: 721–737.
Hounslow, A.W. and Moore, Jr., J.M., 1967. Chemical petrology of Grenville schists near Fernleigh, Ontario. J. Petrol., 8: 1–28.
Hutcheon, I. and Moore, J.M., 1973. The tremolite isograd near Marble Lake, Ontario. Can. J. Earth Sci., 10: 936–947.
Jackson, J.A., 1987. Active normal faulting and crustal extension. In: M.P. Coward, J.F. Dewey and P.L. Hancock (Editors), Continental Extensional Tectonics. Geol. Soc. London Spec. Publ., 28: 3–17.
Jackson, J.A., White, N.J., Garfunkel, Z. and Anderson, H., 1988. Relations between normal-fault geometry, tilting and vertical motions in extensional terrains: an example from the southern Gulf of Suez. J. Struct. Geol., 10: 155–170.
Kohn, M.J. and Spear, F.S., 1990. Two new geobarometers for garnet amphibolites, with applications to southeastern Vermont. Am. Mineral., 75: 89–96.
Kohn, M.J. and Spear, F.S., 1991. Error propagation for barometers, 2. Application to rocks. Am. Mineral., 76: 138–147.
Koziol, A.M. and Newton, R.C., 1988. Redetermination of the anorthite breakdown reaction and improvement of the plagioclase garnet–Al_2SiO_3–quartz geobarometer. Am. Mineral., 73: 216–223.
Kusznir, N.J., Marsden, G. and Egan, S.S., 1991. A flexural-cantilever simple-shear/pure-shear model of continental lithosphere extension: application to the Jeanne d'Arc Basin, Grand Banks and Viking Graben, North Sea. In: A.M. Roberts, G. Yielding and B. Freeman (Editors), The Geometry of Normal Faults. Geol. Soc. London Spec. Publ., 56: 41–60.
Lumbers, S.B., Heaman, L.M., Vertolli, V.M. and Wu, T., 1990. Nature and timing of Middle Proterozoic magmatism in the Central Metasedimentary Belt, Grenville Province, Ontario, In: C.R. Gower, T. Rivers and A.B. Ryan (Editors), Mid-Proterozoic Laurentia–Baltica. Geol. Assoc. Can. Spec. Pap., 38: 243–278.
McEachern, S.J. and van Breemen, O., 1993. Age of deformation within the Central Metasedimentary Belt boundary thrust zone, southwest Grenville Orogen: constraints on the collision of the Mid-Proterozoic Elzevir terrane. Can. J. Earth Sci., 30: 1155–1165.
McKenzie, D., 1978. Active tectonics of the Alpine–Himalayan belt: the Aegean Sea and surrounding regions. Geophys. J. R. Astron. Soc., 55: 217–254.
Mezger, K., van der Pluijm, B.A., Essene, E.J. and Halliday, A.N., 1991. Synorogenic collapse: a perspective from the middle crust, the Proterozoic Grenville Orogen. Science, 254: 695–698.
Mezger, K., Essene, E.J., van der Pluijm, B.A. and Halliday, A.N., 1993. U–Pb geochronology of the Grenville Orogen of Ontario and New York: constraints on ancient crustal tectonics. Contrib. Mineral. Petrol., 114: 13–26.
Miller, E.L., Gans, J.E. and Garing, J., 1983. The Snake Range decollement: an exhumed mid-Tertiary ductile–brittle transition. Tectonics, 2: 239–263.
Moecher, D.P., Essene, E.J. and Anovitz, L.M., 1988. Calculation and application of clinopyroxene–garnet–plagioclase–quartz geobarometers. Contrib. Mineral. Petrol., 100: 92–106.
Moore, Jr., J.M. and Thompson, P.H., 1980. The Flinton Group: a late Precambrian metasedimentary succession in the Grenville Province of eastern Ontario. Can. J. Earth Sci., 17: 1685–1707.
Ontario Geological Survey, 1992a. Bedrock geology of Ontario, southern sheet, map 2544, scale 1:1,000,000.
Ontario Geological Survey, 1992b. Tectonic assemblages of Ontario, southern sheet, map 2578, scale 1:1,000,000.
Parsons, T. and Thompson, G.A., 1993. Does magmatism influence low-angle normal faulting? Geology, 21: 247–250.
Perchuk, L.L. and Aranovich, L.Ya., 1984. Improvement of the biotite–garnet geothermometer: correction for the fluorine content of biotite. Dokl. Akad. Nauk SSSR, 277: 471–475.
Pouchou, J.L. and Pichoir, F., 1984. A new model for quantitative X-ray microanalysis, Part I. application to the analysis of homogeneous samples. Rech. Aérosp., 3: 1–13.
Rathmell, M.A., 1993. Comparison of garnet–biotite, calcite–graphite, and calcite–dolomite thermometry in the Grenville orogen, Canada. M.Sc. Thesis, Univ. of Michigan, Ann Arbor.
Reynolds, S.J., Okaya, D.A., Kruger, J.M., Faulds, J.E. and Potochnik, A., 1994. Three-dimensional geometry of detachment faults and metamorphic core complexes from industry seismic reflection profiles, western and central Arizona. Geol. Soc. Am. Prog. Abstr., 26: A250.
Rivers, T., Martignole, J., Gower, C.F. and Davidson, A., 1989. New tectonic subdivisions of the Grenville Province, Southeast Canadian Shield. Tectonics, 8: 63–84.
Ruppel, C., Royden, L. and Hodges, K.V., 1988. Thermal modeling of extensional tectonics: application to pressure–temperature–time histories of metamorphic rocks. Tectonics, 7: 947–957.
Sager-Kinsman, E.A. and Parrish, R.R., 1993. Geochronology of detrital zircons from the Elzevir and Frontenac terranes, Central Metasedimentary Belt, Grenville Province, Ontario. Can. J. Earth Sci., 30: 465–473.
Scott, R.J. and Lister, G.S., 1992. Detachment faults: evidence for low-angle origin. Geology, 20: 833–836.
Sethuraman, K. and Moore, Jr., J.M., 1973. Petrology of metavolcanic rocks in the Bishop Corners–Donaldson Area, Grenville Province, Ontario. Can. J. Earth Sci., 10: 589–614.
Shackelford, T.J., 1980. Tertiary tectonic denudation of a Mesozoic–early Tertiary(?) gneiss complex, Rawhide Mountains, western Arizona. Geology, 8: 190–194.
Smith, R.B. and Bruhn, R.L., 1984. Intraplate extensional tectonics of the eastern Basin-Range: inferences on structural style from seismic reflection data, regional tectonics, and thermal–mechanical models of brittle–ductile deformation. J. Geophys. Res., 89: 5733–5762.
Spencer, J.E., 1984. Role of tectonic denudation in warping and uplift of low-angle normal faults. Geology, 12: 95–98.
Spencer, J.E. and Chase, C.G., 1989. Role of crustal flexure

in initiation of low-angle normal faults and implications for structural evolution of the Basin and Range Province. J. Geophys. Res., 94: 1765–1775.

Stewart, J.H., 1971. Basin and Range structure — a system of horsts and grabens produced by deep-seated extension. Geol. Soc. Am. Bull., 82: 1019–1044.

Thompson, P.H., 1973. Mineral zones and isograds in 'impure' calcareous rocks, an alternative means of evaluating metamorphic grade. Contrib. Mineral. Petrol., 42: 63–80.

Thompson, P.H. and Leclair, A.D., 1987. Chloritoid–hornblende assemblages in quartz–muscovite pelitic rocks of the Central Metasedimentary Belt, Grenville Province, Canada. J. Metamorph. Geol., 5: 415–436.

van Breemen, O. and Davidson, A., 1988. U–Pb zircon ages of granites and syenites in the Central Metasedimentary Belt, Grenville Province, Ontario: radiogenic age and isotopic studies, Report 2. Geol. Surv. Can. Pap., 88-2: 45–50.

van der Pluijm, B.A. and Carlson, K.A., 1989. Extension in the Central Metasedimentary Belt of the Ontario Grenville: timing and tectonic significance. Geology, 17: 161–164.

van der Pluijm, B.A., Mezger, K., Cosca, M.A. and Essene, E.J., 1994. Determining the significance of high-grade shear zones by using temperature–time paths, with examples from the Grenville orogen. Geology, 22: 743–746.

Wallach, J.L., 1974. Origin of the Hinchinbrooke gneiss and its age relationship to Grenville Group rocks of southeastern Ontario. Geol. Assoc. Can. Annu. Meet., 3rd circ. abstr., St. Johns Newfoundland, 96.

Wernicke, B., 1981. Low angle normal faulting in the Basin and Range Province: nappe tectonics in an extending orogen. Nature, 291: 645–648.

Wernicke, B. and Axen, G.J., 1988. On the role of isostasy in the evolution of normal fault systems. Geology, 16: 848–851.

White, D.J., Easton, R.M., Culshaw, N.G., Milkereit, B., Forsyth, D.A., Carr, S., Green, A.G. and Davidson, A., 1994. Seismic images of the Grenville Orogen in Ontario. Can. J. Earth Sci., 31: 293–307.

Zelt, C.A., Forsyth, D.A., Milkereit, B., White, D.J., Asudeh, I. and Easton, R.M., 1994. Seismic structure of the Central Metasedimentary Belt, southern Grenville Province. Can. J. Earth Sci., 31: 243–254.